Novel Biobased Polylactic Acid/Poly(pentamethylene 2,5-furanoate) Blends for Sustainable Food Packaging

Novel biobased polylactic acid/poly(pentamethylene 2,5-furanoate) blends for sustainable food packaging

Daniele Rigotti[1,2*], Michelina Soccio[3,6], Andrea Dorigato[1,2], Massimo Gazzano[4], Valentina Siracusa[5], Giulia Fredi[1,2] and Nadia Lotti[3,6,7*]

[1] University of Trento, Department of Industrial Engineering, via Sommarive 9 38123 Trento (Italy).

[2] National Interuniversity Consortium of Materials Science and Technology (INSTM), via Giusti 9 50121 Firenze (Italy)

[3] University of Bologna, Department of Civil, Chemical, Environmental, and Materials Engineering, via Terracini 28 40131 Bologna (Italy).

[4] Institute of Organic Synthesis and Photoreactivity, ISOF-CNR, Via Gobetti 101, 40129 Bologna (Italy)

[5] University of Catania, Chemical Science Department, Viale A. Doria 6, 95125 Catania (Italy)

[6] Interdepartmental Center for Industrial Research on Advanced Applications in Mechanical Engineering and Materials Technology, CIRI-MAM, Via Zamboni, 33, 40126 Bologna (Italy).

[7] Interdepartmental Center for Agro-Food Research, CIRI-AGRO, Via Zamboni, 33, 40126 Bologna (Italy).

*Corresponding authors:

Daniele Rigotti (daniele.rigotti-1@unitn.it)

Nadia Lotti (nadia.lotti@unibo.it)

Abstract

Here, solution-cast blends of polylactic acid (PLA) and a novel bioderived poly(pentamethylene 2,5-furanoate) (PPeF) in variable concentrations (1-50 wt%) are prepared and investigated. The characterization of the thin films (thickness 50 μm) highlights that PPeF strongly improves the UV-shielding properties of PLA, with a decrease in transmittance at 275 nm from 47.3 % of neat PLA to 0.77 % with only 1 wt % of PPeF, while the transmittance decrease in the visible region at these PPeF

fractions is marginal, allowing the production of optically transparent films. Despite the complete immiscibility of PLA/PPeF blends, PPeF effectively enhances the ductility of PLA, as the tensile strain at break increases from 7 % of neat PLA to 200 % of the blend with 30 wt% of PPeF. This composition is the most promising also from the gas-barrier point of view, as the gas transmission rates of CO_2 and O_2 drop to one-fourth of those of neat PLA, comparable to those of poly(ethylene terephthalate) (PET). These results highlight that PLA/PPeF blends with PPeF fractions of 30 wt% are very promising for food packaging applications, and their properties could be further enhanced by applying suitable compatibilizers.

Keywords: polylactic acid, poly(pentamethylene 2,5-furanoate), blends, thermal properties, mechanical properties, gas barrier properties.

Introduction

The 21st century is thriving with tremendous economic growth, but at the same time facing irrecoverable ecological damage. This duality could be well expressed by plastics: on the one side, it enables new technological applications thanks to its low cost, low density, durability, and ease of manufacture, but on the other side it can represent a severe environmental threat, especially due to the non-renewable origin and wrong disposal procedures. Plastics production and use are thus associated with non-renewable resource consumption, CO_2 emissions, accumulation of non-degradable waste, nano- and micro-plastics pollution, and emission of toxic substances from incinerators [1]. Plastics' largest market is packaging, continuously growing sustained by a global shift from reusable to single-use containers. Plastics production has reached 360 million tons in 2019, and about 40% of this amount was represented by packaging items [2]. In particular, single-use plastic packaging is a highly valuable material that enables not only the modern lifestyle but even our survival in the event of disasters or pandemics [3]. Plastic packaging can fulfill a wide range of functions including protection of food, drinks, and other perishable goods. Most of the food in supermarkets is contained in plastic foils, and this protective film helps to extend its freshness by keeping it dry or preventing contamination from bacteria. However, petroleum-derived non-biodegradable plastic packaging can constitute a substantial environmental danger. A promising alternative is represented by bioplastics, i.e., bio-based and/or biodegradable plastics [4]. Bioplastics possess similar properties as conventional plastics and offer additional advantages, such as a reduced carbon footprint and additional waste management options. Despite this, the bioplastics market represents today only 0.6 % of the total plastics production [5]. According to the European Bioplastics Association, in 2020 the

worldwide bioplastic production was only 2.11 million tons, out of the 360 million tons of plastics produced annually [6].

One of the most promising biopolymers is poly(lactic acid) (PLA). Its high mechanical properties, good workability, biodegradability, and low toxicity make it the ideal material for the packaging of food and other perishable items [7-9]. PLA can be a homopolymer or a copolymer of L-lactic acid and/or D-lactic acid. Poly(L-lactic acid) (P-L-LA) and poly(D-lactic acid) (P-D-LA) are enantiomerically pure and stereoregular polymers respectively synthesized from L-lactic acid and D-lactic acid and having a melting temperature of approx. 180 °C [10]. The diffusion of PLA in the packaging field is mainly due to the synthesis of low enantiomeric purity statistical copolymers [11]. Despite their interesting mechanical and optical properties, these polymers are relatively brittle, which limits their application to rigid thermoformed packaging [12-15]. To address such shortcomings and improve the ductility and the fracture toughness of PLA, several synthetic plasticizers have been added, such as citrate esters [16], poly(ethylene glycol) [17], and poly(propylene glycol) [18], but the effect of these plasticizers on the material stiffness is generally detrimental [19, 20]. Another option can be blending PLA with tough polymers such as poly(ε-caprolactone) [21, 22] and other biodegradable polymers [23-25], but also in this case a negative side effect is a significant reduction of the stress at yield and the high-temperature dimensional stability. Finding a suitable biobased additive for PLA that improves its ductility without negatively affecting the other mechanical properties is still an open research question.

An interesting class of biopolymers that could be blended with PLA is that of the furanoate polyesters. These polymers represent a commercial biobased alternative to petrochemical terephthalate polyesters such as poly(ethylene terephthalate) (PET) and are synthesized starting from furan-2,5-dicarboxylic acid (FDCA), ranked among the top 12 bio-based building-block chemicals by the Department of Energy in the US [26]. FDCA was first synthesized in 1876, but large-scale production has only become possible since the development of modern bio- and chemical catalysis techniques [26]. FDCA, characterized by an aromatic ring with four carbon atoms and one oxygen atom, can be obtained from biomass-derived sugars and polymerized into poly(ethylene 2,5-furandicarboxylate) (PEF). PEF, which has gained great attention, is referred to as the bio-based polyester of the future not only for its physical-mechanical properties, but also due to the significantly lower energy use and CO_2 emissions compared to PET.

PET replacement by furan counterparts is not limited to PEF, despite its prominent position. Indeed a series of furan-based polyesters, like poly(trimethylene 2,5-furandicarboxylate) (PTF), poly(butylene 2,5-furandicarboxylate) (PBF), poly(pentamethylene 2,5-furandicarboxylate) (PPeF)

or poly(hexamethylene 2,5-furandicarboxylate) (PHF), among others, have a wide range of tunable thermal, mechanical, and gas barrier properties, dependent on the number of methylene groups of the glycol moiety that could enable their use in rigid or flexible packaging [27]. For example, PPeF showed unexpected and interesting properties. In fact, despite being an amorphous rubbery polymer at room temperature, it can be easily processed by compression molding as a freestanding flexible film. PPeF is characterized by exceptional thermal stability (max. degradation rate at 414 °C), mechanical response to tensile test typical of elastomeric materials with instant recovery of the initial shape after breaking, and unexpected exceptional barrier properties to both O_2 and CO_2, comparable to those of ethylene-vinyl alcohol copolymer (EVOH) [27, 28].

Given its interesting mechanical and gas barrier properties, PPeF is a great candidate to be blended with PLA. Despite the growing research interest for furanoate polyesters, very few works can be found in the literature about furan-based blends. Poly(alkylene furanoate) – poly(alkylene terephthalate) blends were studied in depth by Poulopoulou et al. [29, 30]. These polymer families were found poorly miscible if blended in solution, but their miscibility improved by switching from solution blending to high-temperature reactive blending or by using a compatibilizer. On the other hand, blends of furanoate polyesters such as PEF–PBF, PEF–PPF, and PBF–PPF were found homogeneous also by using a solution mixing process [31]. As concerns blends containing furanoate polyesters and PLA, PLA–PBF blends were prepared through solution mixing by Poulopoulou et al., and differential scanning calorimetry (DSC) evidenced blend immiscibility [32]. PLA–PBF blends were also prepared by Long et al. through melt-mixing [33]. They found that adding 5 wt% of PBF to PLA increases its elongation at break from 5 % to 183 %, while tensile strength and elastic modulus remained unaltered. The authors attributed the obtained interesting balance between elastic modulus and toughness to stress-induced crystallization and internal heating through molecular friction of the PBF domains. Conversely, to the best of the authors' knowledge, no papers are found in the literature about physical blends of PLA with PPeF, although the properties of PPeF are very promising in this sense.

Therefore, this work aims to overcome the intrinsic brittleness of PLA by physical blending with PPeF. PLA was blended with different amounts (from 1 wt% to 50 wt%) of PPeF and cast to obtain 50-µm-thick films. The prepared samples were characterized from a microstructural, thermal, and mechanical point of view. The optical transparency and the gas barrier properties were also evaluated and correlated to microstructural features.

Materials and methods

Materials

Poly(lactic acid) (PLA 4032D) in form of granules with density of 1.24 g/cm^3 and melting point of 160°C was supplied by Nature Works LLC. The number average molecular weight of 4032D was 107296 g/mol, its weight average molecular weight was 183177 g/mol and its polydispersity index was 1.71[34]. The content of enantiomer D is in the range 1.4-2.0%[35]. 1,5-pentanediol (PD) (99%), titanium tetrabutoxide (TBT), titanium isopropoxide (TIP), and chloroform (purity ≥99.8%) were Sigma-Aldrich reagent grade products, used without any further purification. 2,5-furandicarboxylic acid (purity=98%) was purchased from CHEMOS GmbH & Co. K.

Poly(pentamethylene furanoate) (PPeF) was prepared by two-stage melt polycondensation, according to the procedure described elsewhere [28]. Briefly, a 200 ml thermostated stirred reactor charged with the reagents FDCA and PD, and the catalysts TBT and TIP (200 ppm), was employed. To improve the diacid solubilization, a key step for the esterification reaction, a 500 mol% excess of glycol was employed. The first stage was carried out for 2 hours at 170 °C under reflux in a nitrogen atmosphere and under stirring (50 rpm); then, the condenser was removed and the gas flow increased to facilitate distillation of water, this stage lasted 1 hour. Afterward, the temperature reaction was increased gradually to 220°C and concurrently the pressure was reduced to 0.01 mbar. The second stage, prolonged until a constant torque value was reached, lasted 2.5 hours. The number average molecular weight of PPeF was 29600 g/mol and its polydispersity index was 2.4 [28].

Sample preparation

Circular polymeric films with a diameter of approx. 11 cm and a thickness of approx. 50 μm were prepared by solution mixing and casting. Solution mixing was chosen to avoid any possible transesterification reactions occurring at elevated temperatures during melt mixing [31]. PLA and PPeF were completely dissolved in chloroform under magnetic stirring at 40 °C for 3 hours, to obtain solutions with PPeF contents ranging from 0 to 50 wt%. Air bubbles were removed in an ultrasonic bath for 5 minutes. The resulting solutions were then cast in a Petri dish and the solvent was let to evaporate first at room temperature for 24 hours and then in a ventilated oven at 40° C for 4 hours. Before being tested, samples were conditioned at 22 °C and 50% of humidity for at least 24 h. Samples were designated as PLA_PPeFx, where x represents the amount of PPeF in wt%. The list of the prepared samples is reported in **Table 1**. A neat PPeF film was also produced for comparison, but it was very difficult to remove from the glass Petri dish. Therefore, a small sample was obtained by

casting onto a Teflon-covered Petri dish, which was subjected to microstructural and optical characterization.

Table 1. List of the prepared samples with nominal weight compositions.

Sample	PLA content (wt%)	PPeF content (wt%)
PLA	100	0
PLA-PPeF1	99	1
PLA-PPeF3	97	3
PLA-PPeF5	95	5
PLA-PPeF20	80	20
PLA-PPeF30	70	30
PLA-PPeF50	50	50

Experimental techniques

The microstructural characterization of the prepared samples was carried out by a JEOL high-resolution Field Emission Scanning Electron Microscope (FE-SEM), operating at an accelerating voltage of 5 kV, analyzing the cryo-fractured cross-section after the deposition of a platinum/palladium conductive coating. The optical transparency of the obtained films was evaluated by a Jasco 570 UV-VIS-NIR spectrophotometer (Easton, MD, USA), determining the energy absorbed in a spectral wavelength range from 250 to 800 nm at a scanning rate of 200 nm/min. In this way, the relative transmittance (T%) of the films over the considered wavelength range was determined. The transparency of the obtained films was qualitatively evaluated with a Canon Eos 550D camera, with a focal length of 135 mm at approx. 25 cm from the specimen.

The thermal stability of the prepared blends was investigated through thermogravimetric analysis (TGA), by using a TA instrument TGA Q5000 machine between 30 °C and 700 °C, at 10 °C/min, under a nitrogen flow of 150 ml/min. The maximum degradation rate temperature (T_d) was estimated from the peak of mass loss derivative curves. Calorimetric measurements were conducted by using a Perkin Elmer DSC6 instrument. In the typical setup, the external block temperature control was set at -70 °C and weighed samples of about 10 mg were heated up to 40 °C above melting temperature at a rate of 20 °C/min (first scan), held there for 3 min, and then rapidly quenched (about 100 °C/min) to -70 °C. Finally, they were reheated from -70 °C to a temperature well above the melting point of the sample at a heating rate of 20 °C/min (second scan). The heat of cold crystallization (ΔH_{cc}) and

the heat of fusion (ΔH_m) of the crystalline phase were calculated from the total areas of the DSC exotherm and endotherm, respectively. These data have been used to calculate the degree of crystallinity ($X_{c,DSC}$) as reported in Equation (1)

$$X_{c,DSC} = (\Delta H_m - \Delta H_{cc}) \cdot 100 / (\Delta H_0 \cdot w_{PLA}) \quad (1)$$

where ΔH_0 is the melting enthalpy of fully crystalline PLA, equal to 93.7 J/g, and w_{PLA} is the weight fraction of PLA in each blend.

Wide angle X-ray scattering (WAXS) patterns of polymeric films were carried out by using a PANalytical X'PertPro diffractometer equipped with a fast solid-state X'Celerator detector and a copper target (l ¼ 0.15418 nm). Spectra were acquired in the 5-60° 2θ interval, by collecting data for 100 s at each 0.10° step. The indices of crystallinity (X_c) were evaluated from the XRD profiles by the ratio between the crystalline diffraction area (A_c) and the total area of the diffraction profile (A_t), $X_c = A_c/A_t$. The amorphous was modeled as a bell-shaped peak baseline. Non-coherent scattering was taken into consideration.

Quasi-static tensile tests were performed on ISO 527 1BA specimens by using an Instron 5969 electromechanical testing machine equipped with a 100 N load cell, operating at a crosshead speed of 10 mm/min. According to ISO 527 standard, the elastic modulus was measured as the secant modulus between strain levels of 0.05% and 0.25%. At least five specimens for each sample were tested at 22 °C and relative humidity of 50%. Impact tests were performed by using a pendulum provided by Ceast. Tensile impact configuration was adopted on ISO 527 1BA specimens. The data acquisition frequency was 200 kHz. Samples were tested at 22 °C and relative humidity of 50%, by imposing an impact speed of 2.14 m/s and maximum energy at impact of 5 J. At least five specimens were tested for each composition.

Gas barrier properties were determined by a manometric method using a Permeance Testing Device, type GDP-C (Brugger Feinmechanik, GmbH, Munich, Germany), according to ASTM 1434-82 (Standard test Method for Determining Gas Permeability Characteristics of Plastic Film and Sheeting), DIN 53 536 in compliance with ISO/DIS 15 105-1 and according to Gas Permeability Testing Manual (Registergericht München HRB 77020, Brugger Feinmechanik GmbH). After preliminary high vacuum desorption of the lower analysis chambers, the upper chamber was filled with the gas test, at ambient pressure. A pressure transducer, set in the lower chamber, continuously records the increase in gas pressure as a function of time. The gas transmission rate (GTR, in $cm^3 \cdot m^{-2} \cdot d^{-1} \cdot bar^{-1}$) was determined by considering the rate of pressure increase and the volume of the device. Permeability was normalized by sample thickness. The operative conditions were: gas stream of 100

$cm^3 \cdot min^{-1}$; 0% RH of gas test, food grade; sample area of 78.5 cm^2 (standard measurement area). Films were analyzed at 23°C (standard temperature of analysis). Gas transmission measurements were performed at least in triplicate and the mean value is presented as average ± standard deviation. Method A was used for the analysis, as reported in the literature [36, 37], with the evacuation of upper/lower chambers. Sample temperature was set by an external thermostat Haake-Circulator DC10-K15 type (Thermo Fisher Scientific, Waltham, MA, USA).

Results and discussion

The morphology of polymer blends thin films depends on various factors, such as blend composition, film thickness, solvent, temperature, chain end group, substrate, polymer structure and molecular weight of polymer, etc [38]. **Figure 1** shows the SEM micrographs of cryogenically fractured cross-sections of the prepared blends. The micrographs provide interesting information on the blend morphology and highlight the extent of the phase separation as a function of the PPeF content. The fracture surface of neat PLA and neat PPeF shows a smooth and uniform surface, which demonstrates that the adopted preparation technique allows obtaining films with uniform morphology and thickness. In all PLA/PPeF blends, PPeF is present as spheroidal domains distributed in the PLA matrix. The interfacial adhesion is rather poor and some interfacial debonding is present in all compositions. In future works, we will aim at improving the interfacial adhesion by including suitable compatibilizers. The size of PPeF domains increases with the PPeF concentration, being 0.57 ± 0.08 μm for PLA_PPeF1, 1.04 ± 0.17 μm for PLA_PPeF5, 2.2 ± 1.9 μm for PLA_PPeF30 and 4.9 ± 3.1 μm for PLA_PPeF50 (calculated with Image J v.1.50i), and their shape varies from spherical to ovoid. The sample with the highest investigated PPeF concentration, i.e., PLA_PPeF50, shows a clear separation between PLA and PPeF, and the film appears as formed of two layers, one constituted by PLA matrix with oval PPeF domains, and the other constituted by a PPeF matrix with big and spherical PLA domains. Such phase separation, with the top area enriched only in one polymer, while exhibiting depletion in the other polymer and *viceversa*, with the nucleation and growth of the minority phase, was already seen in literature[39, 40] and numerical simulated taking into account the kinetics (evaporation rate and diffusion coefficients) and the thermodynamics (parameters that define the free energy) of the system[41].

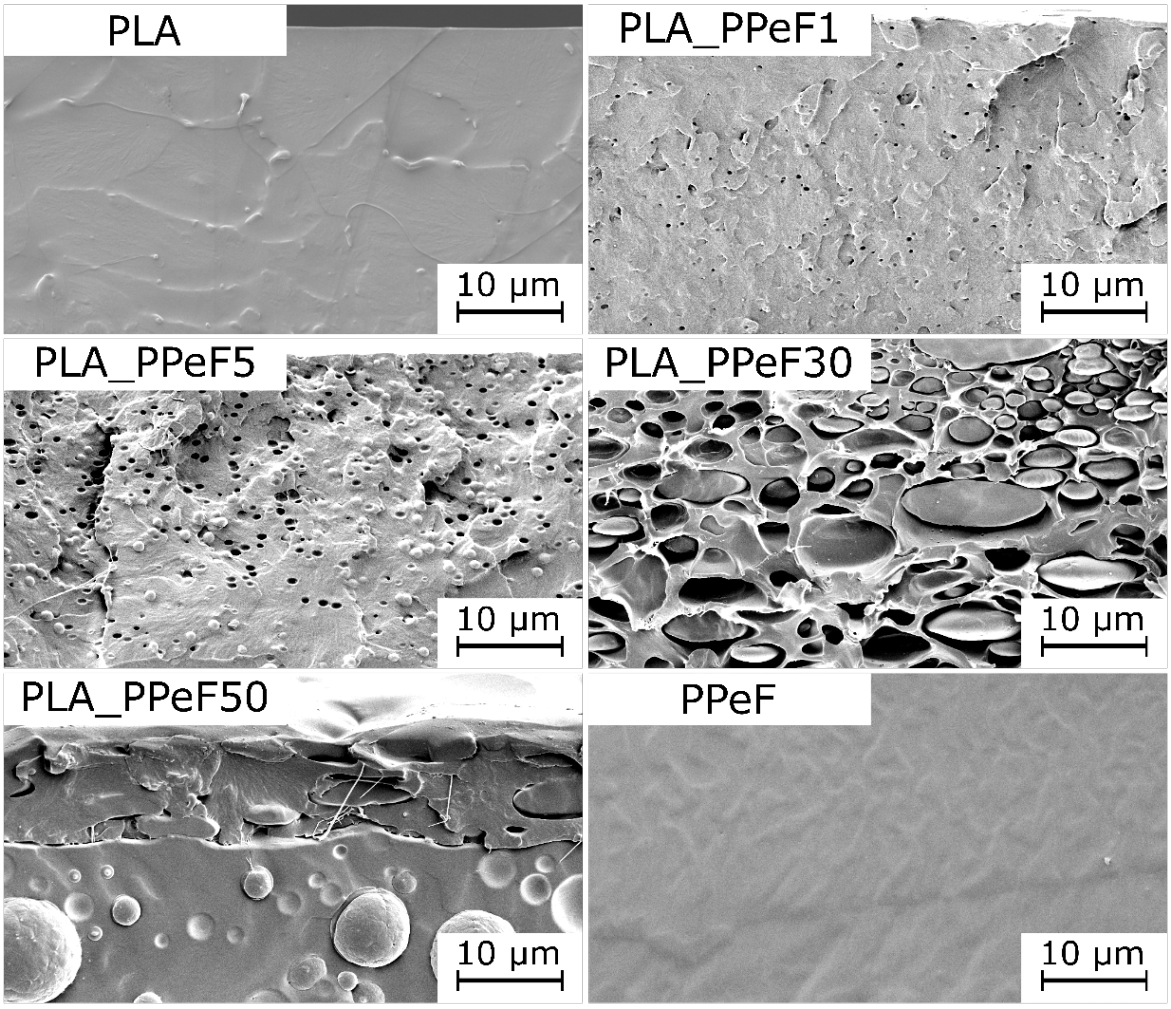

Figure 1. SEM micrographs of the cryofractured cross-sections of the prepared films.

Optical transparency of food packaging in the visible range is a very important property, as it may affect the customer perception of food quality and freshness [42]. Therefore, the optical properties of the prepared films have been studied by optical transmittance measurements in the wavelength range 200-800 nm, and **Figure 2** shows the transmittance curves for all blends. Neat PLA shows good transparency in both UV and visible regions, with transmittance values higher than 40 % for wavelengths above 250 nm and higher than 80 % for wavelengths above 500 nm, in good agreement with data from the literature [43]. If the transparency in the visible range is positive for food packaging materials, the same cannot be said for the transparency to UV radiation, which may accelerate food degradation and decrease the shelf life [42, 44, 45]. Neat PPeF has strong absorption in the UV region, probably due to the UV absorption behavior of furan rings conjugated with carbonyl groups [46]. For the prepared blends, PPeF strongly contributes to improving the UV-shielding properties of PLA. In fact, an amount of PPeF as small as 1 wt% promotes a strong decrease in transmittance in UVC and

UVB regions (225-325 nm). Similar effects have been observed in a previous work of our group on blends of PLA with poly(dodecylene 2,5-furandicarboxylate) [47]. On the other hand, the decrease in transmittance of PLA_PPeF1 compared to neat PLA in the visible range is more modest. For example, the transmittance values for PLA and PLA_PPeF1 at 275 nm are 47.3 % and 0.77 %, respectively, while those at 550 nm are 81.7 % and 74.6 %, respectively. An increase in the PPeF content promotes a further transmittance decrease in the whole investigated wavelength region, which is probably related to the immiscibility between the two phases resulting in micrometric PPeF domains, as evidenced in SEM micrographs (**Figure 1**). However, by considering films with a thickness of 50 µm, the transparency is not dramatically impaired, as can be seen from the photographs reported in **Figure 3**. Therefore, PPeF is an interesting additive for PLA, as it enhances the UV shielding properties and allows retaining optical transparency, which is very promising for the development of smart food packaging.

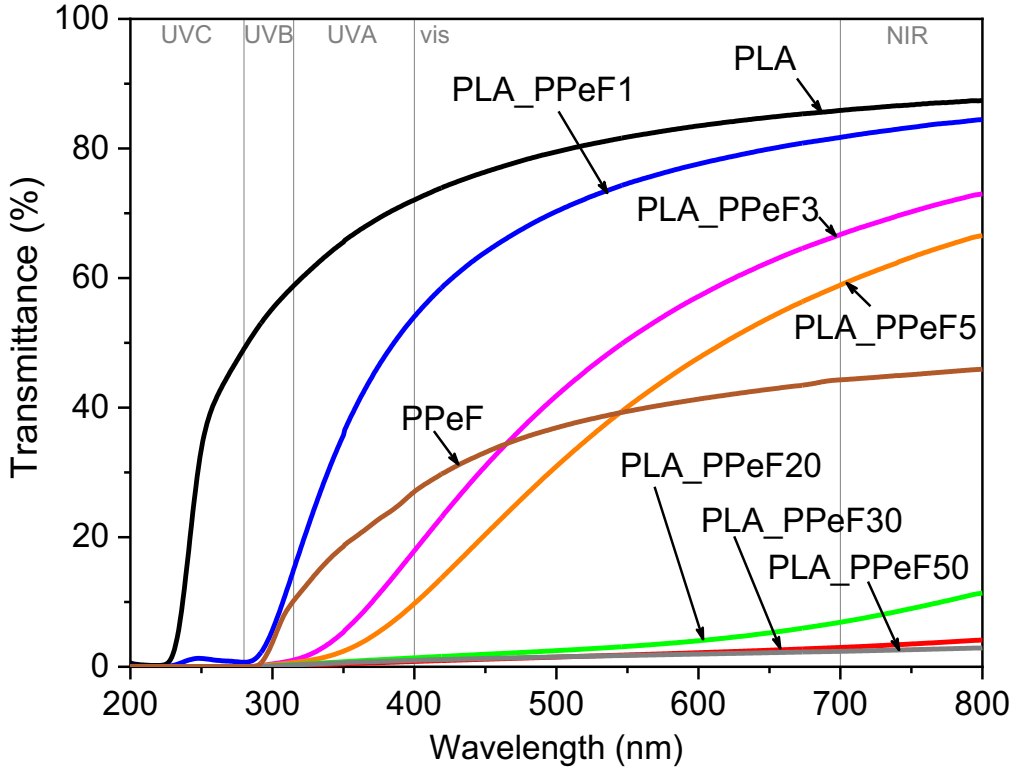

Figure 2. Transmittance of PLA–PPeF films as a function of the wavelength.

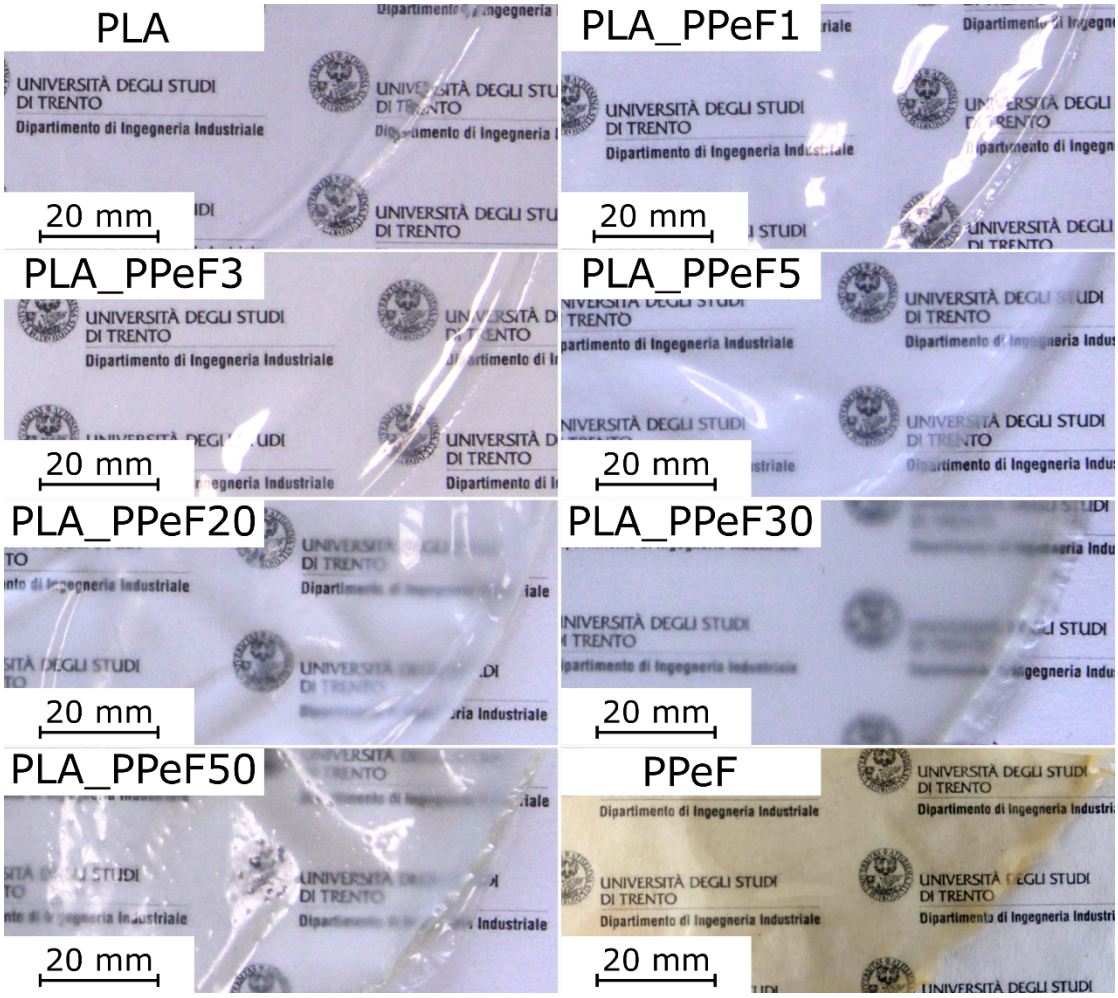

Figure 3. Photographs of the prepared films to qualitatively evaluate the optical transparency.

The phase behavior and the miscibility between the two polymers were investigated through calorimetric measurements. The calorimetric curves of solvent cast blends are shown in **Figure 4a** and the corresponding data are collected in **Table 2**. The DSC traces of all samples present the typical profile of semicrystalline materials, with an endothermic baseline deviation related to glass-to-rubber transition at approx. 54 °C, followed by an endothermic phenomenon associated with the melting of the crystalline phase at approx. 166 °C. The glass transition of neat PLA and blends containing up to 3 wt% of PPeF appears as a sharp jump due to chain shrinkage. The exothermic peak between T_g and T_m is attributable to cold crystallization of the macromolecules which, after glass transition, acquire sufficient energy and mobility to rearrange and crystallize. In all cases, however, $\Delta H_m > \Delta H_{cc}$, proving the semicrystalline nature of all samples. The crystallinity degree of PLA developed in the cooling step from the molten state is slightly higher than that of neat PLA for the samples containing up to 20 wt% of PPeF, then becoming significantly lower for the blends richest in PPeF (PLA_PPeF30 and PLA_PPeF50), as observable from the values of $X_{c,DSC}$ reported in **Table 2**. This suggests that,

whereas small fractions of PPeF can increase the crystallization kinetics of PLA, large PPeF fractions produce the opposite effect. Similar results can be observed for cold crystallization: T_{cc} increases with the PPeF concentration, indicating that the cold crystallization of PLA is somehow hampered by PPeF, when present in large fractions. On the other hand, the melting temperature of PLA does not vary with the composition, the value exactly corresponding to the melting temperature of neat PLA (166 °C), which is a sign of blend immiscibility. The immiscibility is also confirmed by the measured glass transition temperatures, which are found in the blends at temperatures corresponding to the T_g of the two parent homopolymers. For blends containing up to 20% of PPeF, only the glass transition of PLA is visible, which occurs at the typical temperature of PLA homopolymer (54 °C). With a PPeF content above 20 wt%, the thermograms also show the glass transition of PPeF as an endothermic signal at approx. 13 °C, regardless of the composition. Lastly, for the blend with a PPeF content of 20-50 wt%, an additional endothermic peak can be observed just above the T_g of PLA, whose intensity increases with the amount of PPeF. The peak temperature corresponds to the melting temperature of the PPeF crystal phase [48]. The associated heat cannot be estimated because of the overlapping with the glass transition phenomenon of PLA. Therefore, such blends are composed of an immiscible amorphous phase and coexistence of PLA and PPeF crystal phases.

The microstructure and the crystallinity of the prepared blends have been evaluated also through XRD analysis. **Figure 4b** shows the XRD profiles of the prepared samples, together with those of α-PLA and PPeF homopolymers, for reference [48, 49]. All samples show typical profiles of semicrystalline materials, with sharp peaks of the crystal phases overlapped to a bell-shaped background of the amorphous phase. PLA diffraction profile shows two main peaks, at 16.6° (1 1 0 / 2 0 0) and 19.0° (2 0 3 / 1 1 3), and additional peaks at 14.7° (0 1 1) and 22.3° (2 1 1) [49, 50]. These last two signals, although minor, indicate that the crystal phase developed in PLA and all blends is α-PLA. The same reflections also dominate the diffraction patterns of all blends except PLA-PPeF50, which instead only shows the reflections typical of PPeF crystals [48], but the broad halos may hide a minor amount of crystalline PLA phase. The diffraction profiles of PLA_PPeF20 and PLA_PPeF30 samples show diffraction peaks of both PLA and PPeF crystals, which indicates the presence of both crystal phases. These diffractograms also give information on the total crystallinity of the samples, which can be calculated as the ratio between the areas below the peaks of the crystal phases and the total area under the diffraction pattern. The crystallinity index calculated in this way ($X_{c,WAXS}$, **Table 2**) is low (6-8 %) for PLA and PLA-PPeF50, while it is generally higher for the remaining samples (18-27 %), in good agreement with DSC results.

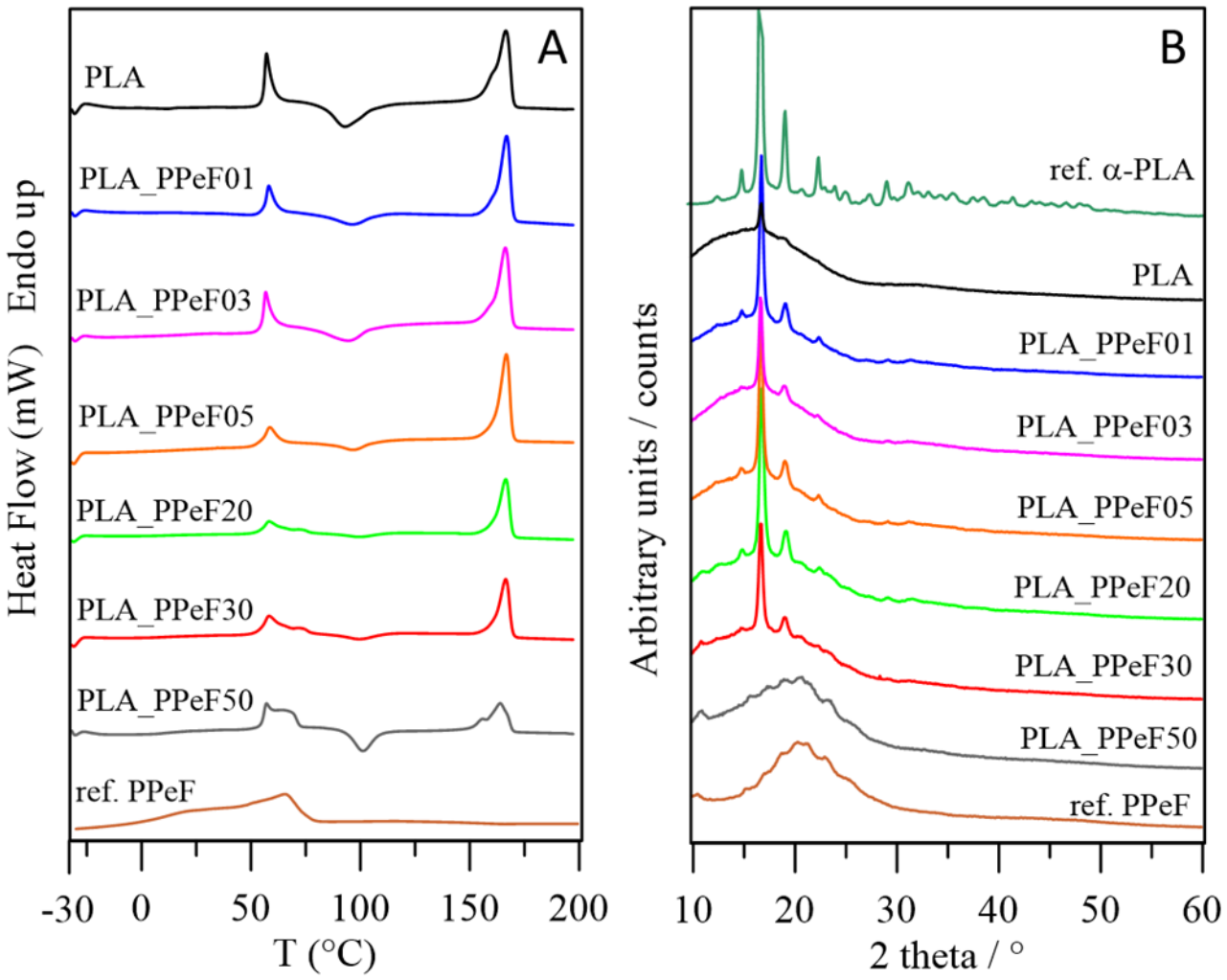

Figure 4. (a) DSC thermograms on the prepared samples (first heating scan); (b) WAXS profiles the prepared samples. Diffraction profiles of α-PLA and PPeF homopolymers are added for comparison.

Table 2. Results of DSC tests on the prepared samples (first heating scan) and degree of crystallinity calculated by WAXS.

Sample	T_g (°C)	Δc_p (J/g°C)	$T_{m,PPeF}$ (°C)	$T_{cc,PLA}$ (°C)	$\Delta H_{cc,PLA}$ (J/g)	$T_{m,PLA}$ (°C)	$\Delta H_{m,PLA}$ (J/g)	$X_{c,DSC}$ (%)	$X_{c,WAXS}$ (%)
PLA	54	0.43	-	93	24	166	39	16	6
PLA_PPeF1	54	0.42	n.d.	95	13	166	34	23	27
PLA_PPeF3	54	0.43	n.d.	94	19	166	35	18	14
PLA_PPeF5	53	0.39	n.d.	96	9	166	30	24	26
PLA_PPeF20	54	n.d.	67	98	3	166	25	29	25
PLA_PPeF30	13; 56	0.11; n.d.	67	99	16	166	23	11	12

PLA_PPeF50	13; 55	0.17; n.d.	67	101	14	164	17	6	8

T_g = glass transition temperature; Δc_p = specific heat increment associated with the glass transition of the amorphous phase; $T_{m,PPeF}$ = melting temperature of PPeF; $T_{cc,PLA}$ = cold crystallization temperature of PLA; $\Delta H_{cc,PLA}$ = cold crystallization enthalpy of PLA; $T_{m,PLA}$ = melting temperature of PLA; $\Delta H_{m,PLA}$ = melting enthalpy of PLA; $X_{c,DSC}$ = crystallinity degree of PLA calculated by DSC; $X_{c,WAXS}$ = crystallinity degree of PLA calculated by WAXS; n.d. = not detectable; - = not applicable.

The mechanical properties of the prepared films were evaluated with quasi-static tensile tests and tensile impact tests. Representative stress-strain curves from quasi-static tensile tests are reported in **Figure 5a**, while the most important results are summarized in **Table 3**. The elastic modulus measured on neat PLA is 1270 MPa, and it generally decreases with an increase in the PPeF amount. For example, PLA_PPeF20 has an average modulus of 880 MPa (-30 % compared to neat PLA), and PLA_PPeF50 shows a modulus of 389 MPa (-70 %). A similar trend can be observed also for the stress at yield (σ_y) and stress at break (σ_b). Again, the drop in mechanical strength is particularly severe for PLA_PPeF50. This drop in the mechanical properties can be related to the poor compatibility between the two phases and the low mechanical strength of neat PPeF ($\sigma_b = 6.1 \pm 0.5$ MPa) [28] and it is commonly reported in literature when PLA is mixed with another phase[51-53]. Conversely, the strain at break (ε_b) of the prepared blends strongly increases with the PPeF concentration, reaching a maximum of 202 % for PLA_PPeF30, with a 30-fold increase compared to neat PLA. Such a considerable increase in ε_b associated with a more modest reduction in stiffness and strength was found also by Long et al. in immiscible PLA/PBF blends containing up to 20 wt% of PBF [33]. They suggested that PLA could be dynamically toughened and strengthened during the elongation process by the synergistic effect of a plastic-rubber transition and a strain-induced crystallization in the PBF domains, which have a T_g close to room temperature. Unlike PBF, PPeF has a T_g below room temperature and is almost entirely amorphous due to the odd number of carbon atoms in the glycol subunit [54], which could further enhance the effect observed by Long et al. Similar results were also found by previous research of our group, dealing with films and fibers of PLA blended with furanoate polyesters with varying alkyl chain length, containing an even number (from 4 to 10) of carbon atoms [47, 55, 56]. Those works showed that a small fraction (5-10 wt%) of any of the considered furanoate polyesters promoted a remarkable increase in tensile strain at break and fracture toughness, and this effect was particularly evident with furanoate polyesters with longer diols, having a T_g below room temperature. This effect, which requires further investigation to be fully comprehended, is very interesting as it addresses one of the main drawbacks of PLA, i.e., brittleness, and opens new strategies to produce PLA-based films with balanced properties.

These results are in good agreement with those of the tensile impact tests. As shown in **Figure 5b**, the specific energy absorbed by the material at fracture is strongly improved by the addition of PPeF.

In fact, the total impact energy increases from 0.067 J/mm^2 of neat PLA up to 0.261 J/mm^2 for PLA-PPeF20, which corresponds to a 4-fold increase. With a PPeF content of 30 wt%, the absorbed energy drops to 0.114 J/mm^2, while the sample PLA_PPeF50 was too brittle to be tested in impact conditions. The results of the mechanical tests highlight that the addition of a proper amount of PPeF to PLA (i.e., 20-30 wt%) strongly increases the strain at break and the impact strength without dramatically deteriorating the stiffness and strength. We believe that the beneficial contribution of PPeF can be maximized by improving the blend compatibilization, which will be object of future studies.

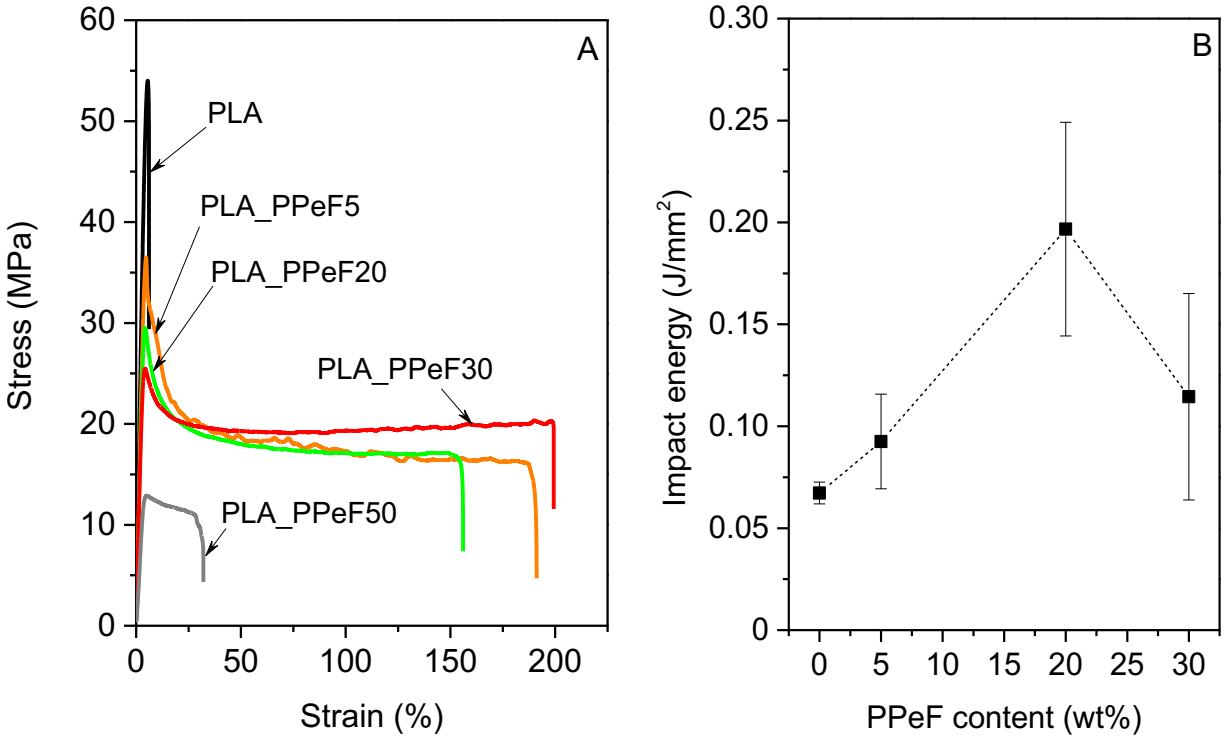

Figure 5. (a) Representative stress-strain curves from quasi-static tensile tests on the prepared samples; (b) Specific total impact energy from tensile impact tests on the prepared blends

Table 3. Mechanical properties from quasi-static tensile tests on the prepared samples.

Sample	Elastic modulus (MPa)	Stress at yield (MPa)	Stress at break (MPa)	Strain at break (%)
PLA	1270 ± 60	52.4 ± 2.3	47.5 ± 4.6	7 ± 2
PLA_PPeF5	984 ± 55	35.9 ± 1.8	20.5 ± 3.8	184 ±178
PLA_PPeF20	880 ± 34	29.2 ± 0.9	19.4 ± 2.0	126 ±105
PLA_PPeF30	764 ± 28	25.7 ± 1.1	20.2 ± 0.9	202 ± 74
PLA_PPeF50	389 ± 44	12.4 ± 0.5	11.0 ± 0.5	33 ± 14

Finally, gas permeation properties have been investigated with dry O_2 and CO_2 gases at 23 °C and 0% of relative humidity. **Figure 6** shows the obtained gas transmission rate (GTR) values normalized by the sample thickness. Data of poly(ethylene terephthalate) (PET), poly(butylene succinate) (PBS), and poly(hydroxybutyrate) (PHB) are also reported for comparison. All samples are more permeable to CO_2 than to O_2, which is common for polymer films, although the CO_2 molecular diameter (3.4 Å) is greater than that of O_2 (3.1 Å). This phenomenon occurs because the affinity between permeating species and permeable matrix, on which the diffusion path depends, is more important than size. Consequently, one can assume the balance between molecular size and bond polarity determines higher permeability, thus greater GRT values, for CO_2 [57-59].

The addition of PPeF to PLA improves its gas barrier performance to both CO_2 and O_2 until a PPeF content of 30 wt%, whereas for PLA_PPeF50 the permeability increases again and returns to values close to those of PLA_PPeF20, which is evident especially for CO_2. The gas barrier performance of a polymer film depends on many factors [59], among which very important are the degree of crystallinity, glass transition temperature, chain polarity and flexibility, and molecular weight and its distribution. Crystallinity plays a key role, as gases cannot diffuse and permeate through highly packed and ordered phases. Consequently, highly crystalline polymers show generally better barrier performance. For the amorphous phase, it is a better gas barrier in the glassy state (below T_g), due to the lower chain mobility and free volume than in the rubbery state. In the present work, the improvement in gas barrier performance with the PPeF content (up to 30 wt%) is likely due to a combination of the increasing degree of crystallinity of PLA and the outstanding gas barrier performance of PPeF [28]. On the other hand, the worse barrier properties of PLA_PPeF50 are probably due to the lower crystallinity and the larger interfacial surface between the two phases, but also a lower film quality, as the low mechanical properties related to the high content of PPeF, that found itself above its own T_g at room temperature, has made it very difficult to obtain a defect-free cast film. Therefore, the presence of small holes or cracks could have determined a worsening in the gas barrier performance. In any case, PLA_PPeF30 is the best performing sample and shows GTR values to O_2 and CO_2 equal to one fourth of those of neat PLA, comparable to those of PET and better than those of other biopolyesters such as PBS and PHB. This evidences that PPeF is very effective in enhancing the gas barrier properties of PLA, which paves the way for the application of PLA/PPeF blends in the food packaging field.

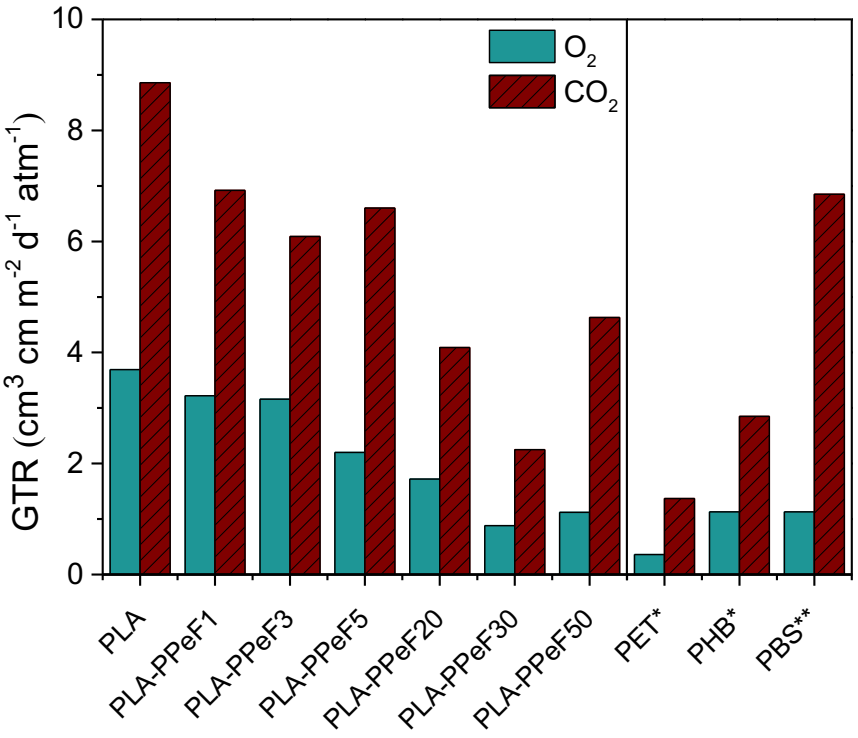

Figure 6. Gas transmission rate (GTR) to O_2 and CO_2 of the prepared films. Data of PET, PHB, and PBS are also reported for reference. *data from [60]; **data from [61].

Conclusions

Physical solution blending of PLA with poly(pentamethylene furanoate) (PPeF) allowed the preparation of a family of new bio-based materials, whose final thermomechanical, optical, and gas barrier properties can be nicely tuned by simply changing the relative amount of the two homopolymers.

Not only did PPeF remarkably enhance the ductility of PLA, but it also provided UV barrier and gas barrier properties, all fundamental for food packaging applications. A content of PPeF as low as 1 wt% considerably reduced the transmittance in the UV region (0.77 % at 275 nm vs 47.3 % of PLA) but not in the visible region (74.6 % at 550 nm vs 81.7 % of neat PLA), thereby allowing the production of transparent films with interesting UV-shielding properties. For the mechanical properties, the sample containing 30 wt% of PPeF showed a strain at break of 202 %, 30 times larger than that of neat PLA, and this was paired with a modest decrease in stiffness and strength. This sample also showed remarkable gas barrier performance, with GTR values to O_2 and CO_2 equal to one-fourth of those of neat PLA, comparable to those of PET, and slightly better than those of PBS and PHB.

30 wt% of PPeF in the blend revealed to be the optimal amount to effectively address the main shortcomings of PLA, i.e., excessive brittleness and poor gas barrier properties, and this paves the way for the production of very interesting biobased materials for sustainable packaging. It is worth mentioning that these promising results\ have been obtained despite the complete immiscibility between PLA and PPeF. A much greater improvement is expected by mixing the two homopolymers in the melt and using suitable compatibilizers.

Funding

This research activity has been funded by Fondazione Cassa di Risparmio di Trento e Rovereto (CARITRO, Grant number 2020.0265). This publication is based upon work from COST Action FUR4Sustain, CA18220, supported by COST (European Cooperation in Science and Technology).

Synopsis

Blending polylactic acid with bioderived poly(pentamethylene 2,5-furanoate) leads to sustainable, ductile, and transparent films with UV-shielding and gas barrier properties, very interesting for food packaging applications.

Table of contents (graphical abstract)

For Table of Contents Use Only

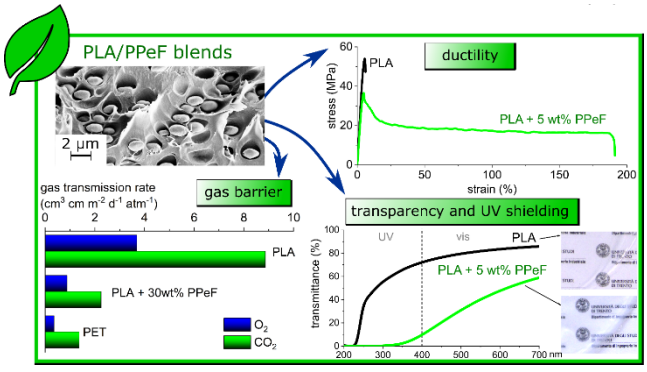

Bibliography

1. Devasahayam, S.; Bhaskar Raju, G.; Mustansar Hussain, C., Utilization and recycling of end of life plastics for sustainable and clean industrial processes including the iron and steel industry. *Materials Science for Energy Technologies* **2019,** *2* (3), 634-646. https://doi.org/10.1016/j.mset.2019.08.002
2. Groh, K. J.; Backhaus, T.; Carney-Almroth, B.; Geueke, B.; Inostroza, P. A.; Lennquist, A.; Leslie, H. A.; Maffini, M.; Slunge, D.; Trasande, L.; Warhurst, A. M.; Muncke, J., Overview of known plastic packaging-associated chemicals and their hazards. *The Science of the total environment* **2019,** *651* (Pt 2), 3253-3268. 10.1016/j.scitotenv.2018.10.015
3. Czigany, T.; Ronkay, F., The coronavirus and plastics. *Express Polym. Lett.* **2020,** *14*, 510-511. 10.3144/expresspolymlett.2020.41
4. Meraldo, A., 4 - Introduction to Bio-Based Polymers. In *Multilayer Flexible Packaging (Second Edition)*, Wagner, J. R., Ed. William Andrew Publishing: 2016; pp 47-52.
5. Niaounakis, M., Recycling of biopolymers – The patent perspective. *European Polymer Journal* **2019,** *114*, 464-475. 10.1016/j.eurpolymj.2019.02.027
6. Konstantopoulou, M.; Terzopoulou, Z.; Nerantzaki, M.; Tsagkalias, J.; Achilias, D. S.; Bikiaris, D. N.; Exarhopoulos, S.; Papageorgiou, D. G.; Papageorgiou, G. Z., Poly(ethylene furanoate- co -ethylene terephthalate) biobased copolymers: Synthesis, thermal properties and cocrystallization behavior. *European Polymer Journal* **2017,** *89*, 349-366. 10.1016/j.eurpolymj.2017.02.037
7. Liu, Z.; Wang, Y.; Wu, B.; Cui, C.; Guo, Y.; Yan, C., A critical review of fused deposition modeling 3D printing technology in manufacturing polylactic acid parts. *The International Journal of Advanced Manufacturing Technology* **2019,** *102* (9-12), 2877-2889. 10.1007/s00170-019-03332-x
8. Pegoretti, A.; Fambri, L.; Migliaresi, C., In vitro degradation of poly(L-lactic acid) fibers produced by melt spinning. *J Appl Polym Sci* **1997,** *64* (2), 213-223. 10.1002/462819970411
9. Tait, M.; Pegoretti, A.; Dorigato, A.; Kaladzidou, K., The effect of filler type and content and the manufacturing process on the performance of multifunctional carbon/poly-lactide composites. *Carbon* **2011,** *49*, 4280-4290.
10. Dorigato, A.; Sebastiani, M.; Pegoretti, A.; Fambri, L., Effect of silica nanoparticles on the mechanical performances of poly(lactic acid). *Journal of Polymers and the Environment* **2012,** *20*, 713–725. 10.1007/s10924-012-0425-6
11. Auras, R.; Lim, L. T., Processing technologies for poly(lactic acid). *Progress in Polymer Science* **2008,** *33*, 820-852. 10.1016/j.progpolymsci.2008.05.004
12. Sun, J.; Shen, J.; Chen, S.; Cooper, M.; Fu, H.; Wu, D.; Yang, Z., Nanofiller Reinforced Biodegradable PLA/PHA Composites: Current Status and Future Trends. *Polymers* **2018,** *10* (5), 505.
13. Swaroop, C.; Shukla, M., Nano-magnesium oxide reinforced polylactic acid biofilms for food packaging applications. *International Journal of Biological Macromolecules* **2018,** *113*, 729-736. https://doi.org/10.1016/j.ijbiomac.2018.02.156
14. Dickmann, M.; Tarter, S.; Egger, W.; Pegoretti, A.; Rigotti, D.; Brusa, R. S.; Checchetto, R., Interface nanocavities in poly (lactic acid) membranes with dispersed cellulose nanofibrils: Their role in the gas barrier performances. *Polymer* **2020,** *202*, 122729. https://doi.org/10.1016/j.polymer.2020.122729
15. Rigotti, D.; Checchetto, R.; Tarter, S.; Caretti, D.; Rizzuto, M.; Fambri, L.; Pegoretti, A., Polylactic acid-lauryl functionalized nanocellulose nanocomposites: Microstructural, thermo-mechanical and gas transport properties. *Express Polym. Lett.* **2019,** *13* (10), 858-876. 10.3144/expresspolymlett.2019.75
16. Labrecque, L. V.; Kumar, R. A.; Dave, V.; Gross, R. A.; McCarthy, S. P., Citrate esters as plasticizers for poly(lactic acid). *J Appl Polym Sci* **1997,** *66*, 1507-1513. 10.1002/1097-4628

17. Jacobsen, S.; Fritz, H. G., Plasticizing polylactide-the effect of different plasticizers on the mechanical properties. *Polymer Engineering ans Science* **2004,** *39* (7), 1303-1310. 10.1002/pen.11517
18. Kulinski, Z.; Piorkowska, E.; Galeski, A.; Masirek, R., Plasticization of semicrystalline poly(l-lactide) with poly(propylene glycol). *Polymer* **2006,** *47*, 7178-7188. 10.1016/j.polymer.2006.03.115
19. Ljungberg, N.; Wesselen, B., The effects of plasticizers on the dynamic mechanical and thermal properties of poly(lactic acid). *Journal of Applied Polymer Science* **2002,** *86*, 1227. 10.1002/app.11077
20. Wypych, G., *Handbook of plasticizers*. ChemTec Publishing: Toronto, 2004.
21. Cabedo, L.; Feijoo, J. L.; Villanueva, M. P.; Lagaron, J. M.; Gimenez, E., Optimization of Biodegradable Nanocomposites Based on aPLA/PCL Blends for Food Packaging Applications. *Macromolecular Symposia* **2006,** *233*, 191-197. 10.1002/masy.200690017
22. Wang, L.; Ma, W.; Gross, R. A.; McCarthy, S. P., Reactive compatibilization of biodegradable blends of poly(lactic acid) and poly(ε-caprolactone). *Polymer Degradation and Stability* **1998,** *59*, 161-168. https://doi.org/10.1016/S0141-3910(97)00196-1
23. Barrows, T. H., Degradable implant materials: A review of synthetic absorbable polymers and their applications. *Clinical Materials* **1986,** *1*, 233-257. https://doi.org/10.1016/S0267-6605(86)80015-4
24. Bastioli, C., *Handbook of biodegradable polymers*. RapraTechnology Limited: Shawbury (UK), 2005.
25. Engelberg, I.; Kohn, J., Physico-mechanical properties of degradable polymers used in medical applications: A comparative study. *Biomaterials* **1991,** *12*, 292-304. https://doi.org/10.1016/0142-9612(91)90037-B
26. Mao, Y.; Zavalij, P., Two furan-2,5-dicarboxylic acid solvates crystallized from dimethylformamide and dimethyl sulfoxide. *Acta Crystallographica Section C Structural Chemistry* **2018,** *74*. 10.1107/S2053229618010471
27. Guidotti, G.; Soccio, M.; García-Gutiérrez, M. C.; Ezquerra, T.; Siracusa, V.; Gutiérrez-Fernández, E.; Munari, A.; Lotti, N., Fully Biobased Superpolymers of 2,5-Furandicarboxylic Acid with Different Functional Properties: From Rigid to Flexible, High Performant Packaging Materials. *ACS Sustainable Chemistry & Engineering* **2020,** *8* (25), 9558-9568. 10.1021/acssuschemeng.0c02840
28. Guidotti, G.; Soccio, M.; García-Gutiérrez, M.-C.; Gutiérrez-Fernández, E.; Ezquerra, T. A.; Siracusa, V.; Munari, A.; Lotti, N., Evidence of a 2D-Ordered Structure in Biobased Poly(pentamethylene furanoate) Responsible for Its Outstanding Barrier and Mechanical Properties. *ACS Sustainable Chemistry & Engineering* **2019,** *7* (21), 17863-17871. 10.1021/acssuschemeng.9b04407
29. Poulopoulou, N.; Kasmi, N.; Bikiaris, D. N.; Papageorgiou, D. G.; Floudas, G.; Papageorgiou, G. Z., Sustainable Polymers from Renewable Resources: Polymer Blends of Furan-Based Polyesters. *Macromolecular Materials and Engineering* **2018,** *303* (8), 1800153. 10.1002/mame.201800153
30. Poulopoulou, N.; Kasmi, N.; Siampani, M.; Terzopoulou, Z. N.; Bikiaris, D. N.; Achilias, D. S.; Papageorgiou, D. G.; Papageorgiou, G. Z., Exploring Next-Generation Engineering Bioplastics: Poly(alkylene furanoate)/Poly(alkylene terephthalate) (PAF/PAT) Blends. *Polymers (Basel)* **2019,** *11* (3). 10.3390/polym11030556
31. Poulopoulou, N.; Pipertzis, A.; Kasmi, N.; Bikiaris, D. N.; Papageorgiou, D. G.; Floudas, G.; Papageorgiou, G. Z., Green polymeric materials: On the dynamic homogeneity and miscibility of furan-based polyester blends. *Polymer* **2019,** *174*, 187-199. 10.1016/j.polymer.2019.04.058
32. Poulopoulou, N.; Kantoutsis, G.; Bikiaris, D. N.; Achilias, D. S.; Kapnisti, M.; Papageorgiou, G. Z., Biobased Engineering Thermoplastics: Poly(butylene 2,5-furandicarboxylate) Blends. *Polymers (Basel)* **2019,** *11* (6). 10.3390/polym11060937

33. Long, Y.; Zhang, R. Y.; Huang, J. C.; Wang, J. G.; Jiang, Y. H.; Hu, G. H.; Yang, J.; Zhu, J., Tensile Property Balanced and Gas Barrier Improved Poly(lactic acid) by Blending with Biobased Poly(butylene 2,5-furan dicarboxylate). *Acs Sustainable Chemistry & Engineering* **2017,** *5* (10), 9244-9253. 10.1021/acssuschemeng.7b02196
34. Kmetty, Á.; Litauszki, K., Development of Poly (Lactide Acid) Foams with Thermally Expandable Microspheres. **2020,** *12* (2), 463.
35. Standau, T.; Zhao, C.; Murillo Castellón, S.; Bonten, C.; Altstädt, V., Chemical Modification and Foam Processing of Polylactide (PLA). *Polymers* **2019,** *11* (2), 306.
36. Siracusa, V. *Food Packaging Permeability Behaviour: A Report*; 1687-9422 1687-9430; 2012; pp 1-11.
37. *Gas Permeability Testing Manual, Registergericht Munchen HRB 77020, Brugger Feinmechanik GmbH*. 2008.
38. Cui, L.; Ding, Y.; Li, X.; Wang, Z.; Han, Y., Solvent and polymer concentration effects on the surface morphology evolution of immiscible polystyrene/poly(methyl methacrylate) blends. *Thin Solid Films* **2006,** *515* (4), 2038-2048. https://doi.org/10.1016/j.tsf.2006.04.045
39. Yeganeh, J. K.; Goharpey, F.; Foudazi, R., Anomalous phase separation behavior in dynamically asymmetric LCST polymer blends. *RSC Advances* **2014,** *4* (25), 12809-12825. 10.1039/C3RA47299J
40. Xue, L.; Zhang, J.; Han, Y., Phase separation induced ordered patterns in thin polymer blend films. *Progress in Polymer Science* **2012,** *37* (4), 564-594. https://doi.org/10.1016/j.progpolymsci.2011.09.001
41. Wodo, O.; Ganapathysubramanian, B., How do evaporating thin films evolve? Unravelling phase-separation mechanisms during solvent-based fabrication of polymer blends. **2014,** *105* (15), 153104. 10.1063/1.4898136
42. Yadav, M.; Chiu, F. C., Cellulose nanocrystals reinforced kappa-carrageenan based UV resistant transparent bionanocomposite films for sustainable packaging applications. *Carbohydr Polym* **2019,** *211*, 181-194. 10.1016/j.carbpol.2019.01.114
43. Roy, S.; Rhim, J. W., Preparation of bioactive functional poly(lactic acid)/curcumin composite film for food packaging application. *Int J Biol Macromol* **2020,** *162*, 1780-1789. 10.1016/j.ijbiomac.2020.08.094
44. Lei, Y.; Mao, L.; Yao, J.; Zhu, H., Improved mechanical, antibacterial and UV barrier properties of catechol-functionalized chitosan/polyvinyl alcohol biodegradable composites for active food packaging. *Carbohydr Polym* **2021,** *264*, 117997. 10.1016/j.carbpol.2021.117997
45. Wang, Y. Y.; Yu, H. Y.; Yang, L.; Abdalkarim, S. Y. H.; Chen, W. L., Enhancing long-term biodegradability and UV-shielding performances of transparent polylactic acid nanocomposite films by adding cellulose nanocrystal-zinc oxide hybrids. *Int J Biol Macromol* **2019,** *141*, 893-905. 10.1016/j.ijbiomac.2019.09.062
46. Borisova, N. N.; Kul'nevich, V. G., UV spectra of carbonyl-contaiming furan compounds. *Khimiya Geterotsiklicheskikh Soedinenii,* **1973,** *5*, 590-594.
47. Fredi, G.; Jafari, M. K.; Checchetto, R.; Bikiaris, D. N.; Favaro, M.; Dorigato, A.; Pegoretti, A., Multifunctionality of reduced graphene oxide in bioderived polylactide/poly(dodecylene furanoate) nanocomposite films. *Molecules* **2021,** *26* (10), 2398. 10.3390/molecules26102938
48. Martínez-Tong, D. E.; Soccio, M.; Robles-Hernández, B.; Guidotti, G.; Gazzano, M.; Lotti, N.; Alegria, A., Evidence of Nanostructure Development from the Molecular Dynamics of Poly(pentamethylene 2,5-furanoate). *Macromolecules* **2020,** *53* (23), 10526-10537. 10.1021/acs.macromol.0c02297
49. Cocca, M.; Androsch, R.; Righetti, M. C.; Malinconico, M.; Di Lorenzo, M. L., Conformationally disordered crystals and their influence on material properties: The cases of isotactic polypropylene, isotactic poly(1-butene), and poly(l-lactic acid). *Journal of Molecular Structure* **2014,** *1078*, 114-132. 10.1016/j.molstruc.2014.02.038

50. Sasaki, S.; Asakura, T., Helix Distortion and Crystal Structure of the R-Form of Poly(L-lactide). *Macromolecules* **2003,** *36*, 8385-8390.
51. Jompang, L.; Thumsorn, S.; On, J.; Surin, P.; Apawet, C.; Chaichalermwong, T.; Kaabbuathong, N.; O-Charoen, N.; Srisawat, N., Poly(Lactic Acid) and Poly(Butylene Succinate) Blend Fibers Prepared by Melt Spinning Technique. *Energy Procedia* **2013,** *34*, 493-499. 10.1016/j.egypro.2013.06.777
52. Li, Y.; Yao, S.; Han, C.; Yu, Y.; Xiao, L., Ternary blends from biological poly(3-hydroxybutyrate-co-4-hydroxyvalerate), poly(L-lactic acid), and poly(vinyl acetate) with balanced properties. *International Journal of Biological Macromolecules* **2021,** *181*, 60-71. https://doi.org/10.1016/j.ijbiomac.2021.03.127
53. Palai, B.; Biswal, M.; Mohanty, S.; Nayak, S. K., In situ reactive compatibilization of polylactic acid (PLA) and thermoplastic starch (TPS) blends; synthesis and evaluation of extrusion blown films thereof. *Industrial Crops and Products* **2019,** *141*, 111748. https://doi.org/10.1016/j.indcrop.2019.111748
54. Soccio, M.; Martinez-Tong, D. E.; Guidotti, G.; Robles-Hernandez, B.; Munari, A.; Lotti, N.; Alegria, A., Broadband Dielectric Spectroscopy Study of Biobased Poly(alkylene 2,5-furanoate)s' Molecular Dynamics. *Polymers (Basel)* **2020,** *12* (6). 10.3390/polym12061355
55. Fredi, G.; Rigotti, D.; Bikiaris, D. N.; Dorigato, A., Tuning thermo-mechanical properties of poly(lactic acid) films through blending with bioderived poly(alkylene furanoate)s with different alkyl chain length for sustainable packaging. *Polymer* **2021,** *218*, 123527. https://doi.org/10.1016/j.polymer.2021.123527
56. Perin, D.; Rigotti, D.; Fredi, G.; Papageorgiou, G. Z.; Bikiaris, D. N.; Dorigato, A., Innovative Bio-based Poly(Lactic Acid)/Poly(Alkylene Furanoate)s Fiber Blends for Sustainable Textile Applications. *Journal of Polymers and the Environment* **2021**. 10.1007/s10924-021-02161-y
57. Genovese, L.; Gigli, M.; Lotti, N.; Gazzano, M.; Siracusa, V.; Munari, A.; Dalla Rosa, M., Biodegradable Long Chain Aliphatic Polyesters Containing Ether-Linkages: Synthesis, Solid-State, and Barrier Properties. *Industrial & Engineering Chemistry Research* **2014,** *53* (27), 10965-10973. 10.1021/ie5017865
58. Guidotti, G.; Soccio, M.; Siracusa, V.; Gazzano, M.; Salatelli, E.; Munari, A.; Lotti, N., Novel Random PBS-Based Copolymers Containing Aliphatic Side Chains for Sustainable Flexible Food Packaging. *Polymers (Basel)* **2017,** *9* (12). 10.3390/polym9120724
59. Robertson, G. L., Optical, Mechanical and Barrier Properties of Thermoplastics Polymers. In *Food Packaging-Principles and Practice*, 3rd edition ed.; CRC Press - Taylor&Francis Group: Boca Raton, FL, USA, 2013; pp 91–130.
60. Mensitieri, G.; Di Maio, E.; Buonocore, G. G.; Nedi, I.; Oliviero, M.; Sansone, L.; Iannace, S., Processing and shelf life issues of selected food packaging materials and structures from renewable resources. *Trends in Food Science & Technology* **2011,** *22* (2-3), 72-80. 10.1016/j.tifs.2010.10.001
61. Genovese, L.; Lotti, N.; Gazzano, M.; Siracusa, V.; Dalla Rosa, M.; Munari, A., Novel biodegradable aliphatic copolyesters based on poly(butylene succinate) containing thioether-linkages for sustainable food packaging applications. *Polymer Degradation and Stability* **2016,** *132*, 191-201. 10.1016/j.polymdegradstab.2016.02.022